RSC Advances

ROYAL SOCIETY OF CHEMISTRY

www.rsc.org/advances

Cite this: DOI: 10.1039/c0xx00000x

www.rsc.org/xxxxxx

ARTICLE TYPE

Circularly Polarized Luminescence of Biaryl Atropisomers: Subtle but Significant Structural Dependency

Yoko Kitayama,[a] Kazuki Nakabayashi,[a] Takashi Wakabayashi,[a] Nobuo Tajima,[b] Michiya Fujiki,[c]* and Yoshitane Imai[a]*

Received (in XXX, XXX) Xth XXXXXXXXX 20XX, Accepted Xth XXXXXXXXX 20XX
DOI: 10.1039/b000000x

The signs of circularly polarised luminescence and circular dichroism of chiral biaryl fluorophores in the $CHCl_3$-dissolved state (solution state) and the PMMA-film-dispersed state (solid state) were successfully controlled by modifying the internal axial chirality and the axial bonding position of biaryl units.

Introduction

Recently, highly emissive organic fluorophores have received much attention in the fields of organic electroluminescent (EL) devices and optical sensors.[1] In particular, current studies are focused on searching for chiral organic fluorophores enabling circularly polarized luminescence (CPL) with high quantum efficiency.[2] In this context, understanding the inherent chiroptical properties of chiral organic fluorophores in the ground and photoexcited states is necessary for the efficient design of elaborate chiroptical functions, including external bias driven switching and memory. Thus, systematic investigation of the chiroptical properties of biaryl atropisomers is important because biaryls are regarded as the most suitable chromophoric models among numbers of chromophores comprising axial chirality.

To rationally invert the sign of the Cotton CPL signal of a chiral fluorophore, an organic fluorophore with opposite point chirality (stereogenic centers) is needed. However, this approach has practical limitations because enantiopure fluorophore pairs must be isolated. Thus, an elegant approach for fine controlling the CPL sign of chiral fluorophores without use of opposite point chirality is well acknowledged.[3] In recent papers, we demonstrated several novel approaches for facile control of the CPL signs of binaphthyl-based fluorophores possessing the same axial chirality (stereogenic bonds) by changing the dihedral bond angle between two naphthyl units.[4] This facile CPL sign inversion approach is also achievable by modifying steric demanding factors between adjacent binaphthyl units and by choosing external matrices (fluidic solutions, solid polymers, and inorganic salts).[4]

To gain a deeper understanding of how biaryl moiety affects the CPL sign, in this study we focused on a relationship between the internal axial bond position of biaryls with the same (*R*)- and (*S*)-axial chirality and the resulting CPL sign. To this end, we chose three pairs of optically active aryl fluorophores (Scheme 1): (i) (*R*)-(-)-3,3′-diphenyl-2,2′-bi-1-naphthol (VANOL) hydrogen phosphate [(*R*)-**1**] and its (*S*)-analog [(*S*)-**1**] as binaphthyls, (ii) (*R*)-(-)-2,2′-diphenyl-4-biphenanthrol (VAPOL) hydrogen phosphate [(*R*)-**2**] and its (*S*)-analog [(*S*)-**2**] as bisphenanthryls with an axial bonding position similar to (*R*)-**1**, and (iii) (*R*)-(-)-1,1′-binaphthyl-2,2′-diyl hydrogen phosphate [(*R*)-**3**] and its (*S*)-analog [(*S*)-**3**] as a different internal axial bonding position of these biaryls. Herein, we demonstrate for the first time that the CPL sign is determined solely by the internal axial bonding position of these biaryls.

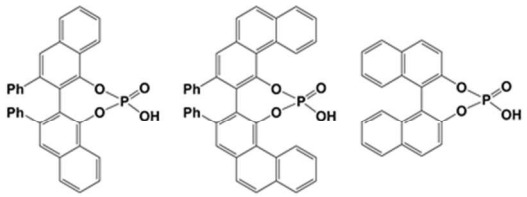

1 2 3

Experimental section

General

Compounds (*R*)-**1** and (*S*)-**1** were prepared using a previously reported method.[5] (*R*)-**2** and (*S*)-**2** were purchased from Sigma-Aldrich Japan (Tokyo, Japan). Chloroform ($CHCl_3$) used for crystallisation and optical measurements was purchased from Wako Pure Chemical Industries (Osaka, Japan).

Measurement of the CPL and PL spectra

Fluorescence spectra and absolute photoluminescence quantum yields in $CHCl_3$ and PMMA film states were measured using an absolute PL quantum yield measurement system (Hamamatsu Photonics C9920-02, Hamamatsu, Japan) under air atmosphere at room temperature. The PMMA films doped with biaryls were prepared using a spin coater at 3000 rpm (Opticoat MS-A100, Mikasa, Tokyo, Japan). The dilute $CHCl_3$ solutions of (*R*)-**1** and

(*R*)-**2** (1.0×10^{-4} M) were excited at 307 and 335 nm, respectively. (*R*)-**1** and (*R*)-**2** in PMMA films were excited at 320 and 330 nm, respectively.

The CPL spectra in $CHCl_3$ solution and PMMA films were measured using a JASCO CPL-200 spectrofluoropolarimeter (Tokyo, Japan) at room temperature. The instrument used a scattering angle of 0° from the excitation of unpolarised, monochromated incident light with a bandwidth of 10 nm. The specimens in PMMA films were prepared analogously to the samples used for the solid-state fluorescence spectra. (*R*)-**1** and (*R*)-**2** at a concentration of 1.0×10^{-4} M in $CHCl_3$ solutions were excited at 307 and 335 nm, respectively. (*R*)-**1** and (*R*)-**2** in PMMA films were excited at 320 and 330 nm, respectively. The CPL spectra were approximated using the simple moving average (SMA) method.

Theoretical calculations

The geometries of (*R*)-**1** and (*R*)-**2** were optimised using the hybrid density functional theory (B3LYP functional).[6] The excitation energies and rotational strengths of the geometry-optimised molecules were calculated using the time-dependent density functional theory[7] with the B3LYP functional. In all the calculations, the cc-pVDZ basis set was used.[8] The program Gaussian03[9] was used for quantum chemical calculations.

Results and discussion

A comparison of unpolarised photoluminescence (PL) properties of (*R*)-**1** and (*R*)-**3**[4a,10] in chloroform ($CHCl_3$) is given in Fig. 1 (lower panel).

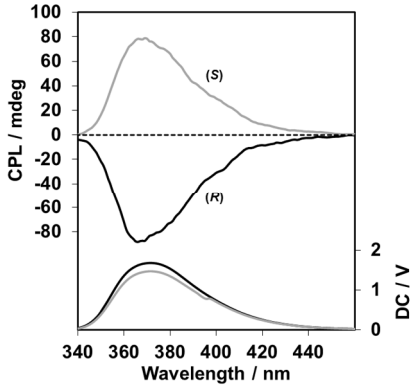

Fig. 1 CPL (upper panel) and PL (lower panel) spectra of (*R*)-**1** (black lines) and (*S*)-**1** (grey lines) in $CHCl_3$ (1.0×10^{-4} M).

The fluorophore (*R*)-**1** in $CHCl_3$ has a PL maximum (λ_{em}) at 372 nm with an absolute value of PL quantum yield (Φ_F) of 0.12 (indicated by black line). The differences in the λ_{em} and Φ_F values between (*R*)-**1** and (*R*)-**3** [λ_{em} = 350 nm and $\Phi_F = 0.29$][4a,10] was calculated. Remarkably, the Φ_F value of (*R*)-**1** was almost half that of (*R*)-**3**. This may arise from thermal deactivation due to higher vibrational modes in (*R*)-**1** than (*R*)-**3**.

As expected, (*R*)-**1** can emit CPL in the order of $|g_{em}| \sim 10^{-3}$, where the dimensionless Kuhn's anisotropy (g_{em}) is defined as $g_{em} = 2(I_L-I_R)/(I_L+I_R)$. The CPL spectrum of (*R*)-**1** in $CHCl_3$ is shown in Fig. 1 (upper panel, black line). Surprisingly, although (*R*)-**1** and (*R*)-**3** commonly possess the same axially chiral binaphthyl units, they exhibit opposite signs in their CPL: a negative CPL sign for (*R*)-**1** and a positive CPL sign for (*R*)-**3** (Fig. 2, black lines for (*R*)-**3**)[11].

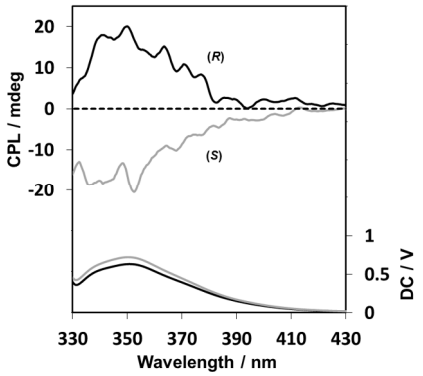

Fig. 2 CPL (upper panel) and PL (lower panel) spectra of (*R*)-**3** (black lines) and (*S*)-**3** (grey lines) in $CHCl_3$ (1.0×10^{-4} M).[11]

To verify whether (*R*)-**1** introduced any artifacts in this CPL spectrum, the CPL spectrum of (*S*)-**1** in $CHCl_3$ was obtained in a similar way (Fig. 1, grey lines). The CPL spectra of (*R*)-**1** and (*S*)-**1** are mirror images of each other. The value of $|g_{em}|$ is ~3.5×10^{-3} for **1**, which is larger than that of **3** ($|g_{em}| \sim 1.5\times10^{-3}$).[10] These results suggest that the CPL sign can be affected by the internal axial bonding position of binaphthyl units as well as by axial chirality.

To elucidate the origin of the CPL reversal, circular dichroism (CD) and UV-Vis absorption spectra of (*R*)-**1** and (*S*)-**1** in $CHCl_3$ were measured and compared to those of (*R*)-**3** and (*S*)-**3**. UV-Vis bands due to π-π* transitions characteristic of naphthyl groups in **1** are clearly observed between 250 and 350 nm (Fig. 3).

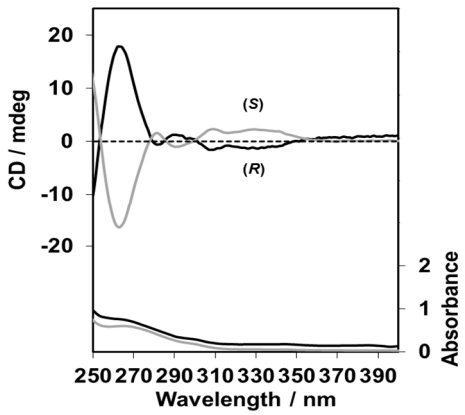

Fig. 3 CD (upper panel) and UV–Vis (lower panel) spectra of (*R*)-**1** (black lines) and (*S*)-**1** (grey lines) in $CHCl_3$ (1.0×10^{-5} M).

The Cotton CD bands of (*R*)-**1** and (*S*)-**1** clearly demonstrate an almost mirror-image relationship due to π-π* transition moments. To quantitatively determine the CD amplitudes, we used the dimensionless Kuhn's anisotropy factor in the ground state, which is defined as $g_{CD} = \Delta\varepsilon/\varepsilon$. The $|g_{CD}|$ value at the first Cotton CD band (λ_{CD} = 343 nm) for **1** is ~3.2×10^{-4}. On the other

hand, the $|g_{CD}|$ value of **3** at the first Cotton CD band (λ_{CD} = 324 nm) is ~1.6 × 10^{-3}.[10] As in the case of CPL spectra, the CD spectra exhibit opposite signs: a negative sign for (*R*)-**1** and a positive sign for (*R*)-**3** (Fig. 4, black lines for (*R*)-**3**)[11].

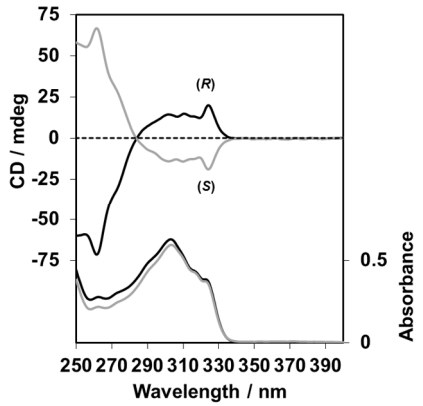

Fig. 4 CD (upper panel) and UV–Vis (lower panel) spectra of (*R*)-**3** (black lines) and (*S*)-**3** (grey lines) in $CHCl_3$ (1.0×10^{-5} M).[11]

The signs of the CPL and the first Cotton CD band of (*R*)-**1** are both negative, while those of (*R*)-**3** are both positive. The sign reversal in the first Cotton CD bands is thus responsible for the reversal in the sign of the CPL bands observed for (*R*)-**1** and (*R*)-**3**.

In the case of (*R*)-**2**, which is an extension of π-conjugation of (*R*)-**1**, (*R*)-**2** in $CHCl_3$ weakly emits at 373 nm (λ_{em}) with Φ_F 0.09 (lower panel in Fig. 5, black line) and shows a negative CPL band (Fig. 5, upper panel, black line). To verify whether any artifacts existed in the CPL spectrum, we obtained the CPL spectrum of (*S*)-**2** in $CHCl_3$ for comparison (grey lines in Fig. 5). Because the CPL spectra of (*R*)-**2** and (*S*)-**2** exhibit an almost mirror-image relationship, the $|g_{em}|$ value for **2** is ~1.3×10^{-3}. Note that CPL signs for (*R*)-**2** and (*R*)-**3** are opposite: a negative for (*R*)-**2** and a positive for (*R*)-**3**.

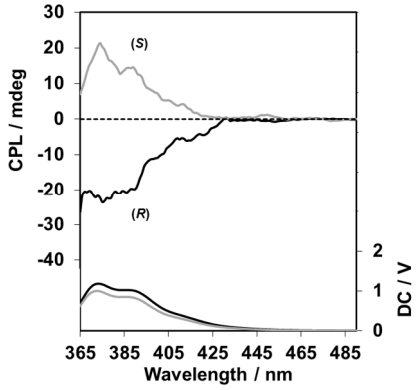

Fig. 5 CPL (upper panel) and PL (lower panel) spectra of (*R*)-**2** (black lines) and (*S*)-**2** (grey lines) in $CHCl_3$ (1.0×10^{-4} M).

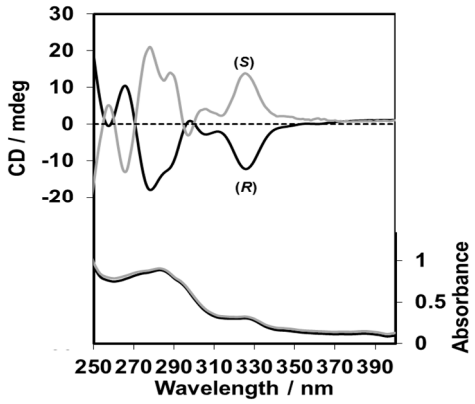

Fig. 6 CD (upper panel) and UV–Vis (lower panel) spectra of (*R*)-**2** (black lines) and (*S*)-**2** (grey lines) in $CHCl_3$ (1.0×10^{-5} M).

The CD and UV-Vis absorption spectra of (*R*)-**2** in $CHCl_3$ are shown in Fig. 6 (indicated by black lines). In contrast to (*R*)-**1**, the characteristic peaks originating from the π-π* transition of the biphenanthryl group in **2** are observed between 260 and 370 nm. To check if there are artefacts in the (*R*)-**2** spectrum, we measured the CD spectrum of (*S*)-**2** in $CHCl_3$ (Fig. 6, grey lines). It is evident that (*R*)-**2** and (*S*)-**2** display an almost mirror-image relationship in their CD spectra. The $|g_{CD}|$ value of the first Cotton CD band (λ_{CD} = 361 nm) is ~3.1×10^{-4}. As expected, (*R*)-**1** and (*R*)-**2** exhibit the same signs in their CD spectra: a negative sign for both (*R*)-**1** and (*R*)-**2**.

To explain the origins of the opposite signs between (*R*)-**1**, (*R*)-**2**, and (*R*)-**3** in their CPL and CD spectra, the equilibrium structures of (*R*)-**1** and (*R*)-**2** were examined theoretically (Fig. 7) and compared with the equilibrium structure of (*R*)-**3** shown previously.[10]

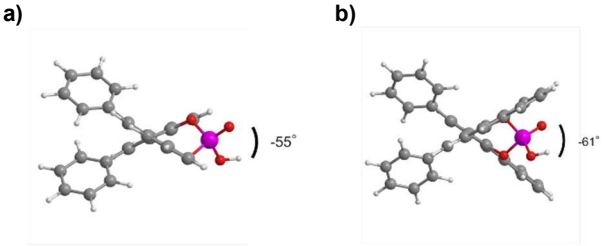

Fig. 7 Theoretically optimized structures of a) (*R*)-**1** and b) (*R*)-**2**.

The dihedral angles θ ((O)C-C-C-C(O)) of (*R*)-**1**, (*R*)-**2**, and (*R*)-**3** are calculated as -55°, -61°, and -53°,[10] respectively. No significant difference in these θ angles between (*R*)-**1**, (*R*)-**2**, and (*R*)-**3** is obtained theoretically, suggesting that the origin of the opposite CPL/CD signs cannot be simply ascribed to different conformations around the central C-C rotational bond.

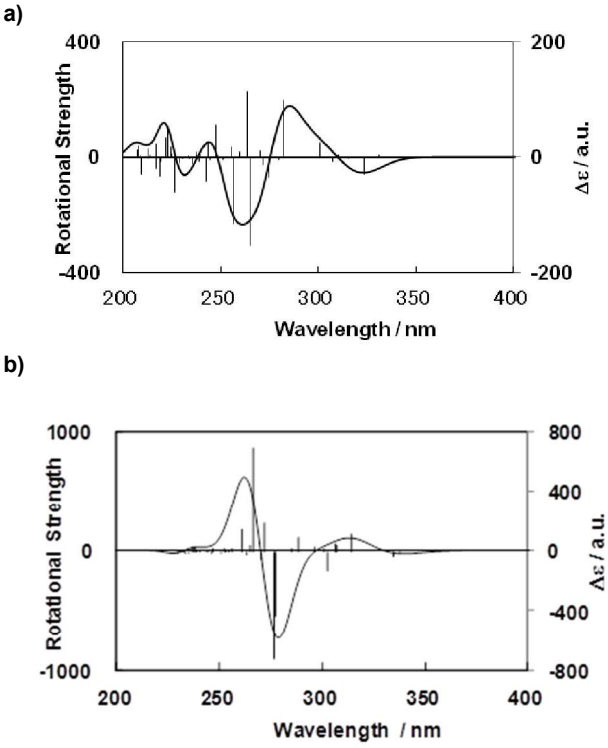

Fig. 8 Calculated excitation wavelengths (λ) and rotational strengths (R) for a) (R)-**1** and b) (R)-**2**. Unit of rotational strength: 10^{-40} erg·esu·cm/G.

The electronic excitation spectra of (R)-**1** and (R)-**2** are employed theoretically as that of (R)-**3** was done previously.[10] Fig. 8 shows calculated rotational strengths of (R)-**1** and (R)-**2** as a function of excitation wavelengths (λ) (Figs. 8a and 8b). These calculations suggest that (R)-**1** and (R)-**2** should have negative CD signals at the long-wavelength edge of the spectra (~330 nm and ~340 nm, respectively). The experimental CD spectra of (R)-**1** and (R)-**2** in $CHCl_3$ are consistent with these theoretical results. The calculated CD intensities at these wavelengths can be explained as a result of non-coplanar monoaryl geometry of these molecules and reflected from the coupling of π-π* electronic transitions over each of the naphthalene and phenanthryl rings. In contrast, (R)-**3** has a weak positive Cotton CD signal at the long-wavelength edge in the CD spectrum (~340 nm).[10] These CD calculations agree well with the experimental CD characteristics.

For practical use as a CPL emitter, a detailed characterization of solid-state chiroptical properties is important. We recently studied the solid-state chiroptical properties of several chiral fluorophores doped into poly(methyl methacrylate) (PMMA) glassy matrices.[4b,4d,10,12] The CPL spectra of (R)-**1** and (R)-**2** dispersed in spin-coated PMMA films clearly exhibit CPL and PL properties, as shown in Figs. 9 and 10 (black lines), respectively. (R)-**1** and (R)-**2** in PMMA films emit at λ_{em} 372 and 376 nm and have Φ_F 0.16 and 0.19, respectively. The CPL spectra between (R)-**1** and (S)-**1,** and between (R)-**2** and (S)-**2** are near mirror images of each other. (R)-**1** and (R)-**2** in PMMA films exhibit CPL in the order of $|g_{em}|$ ~1.7×10^{-3} and ~7.9×10^{-4}, respectively.

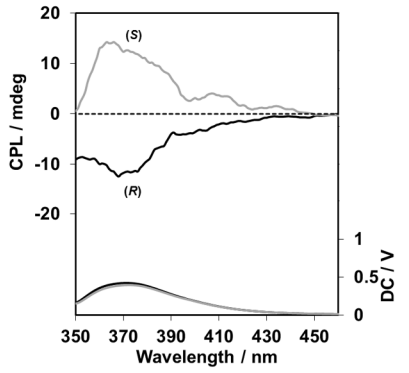

Fig. 9 CPL (upper panel) and PL (lower panel) spectra for (R)-**1** (black lines) and (S)-**1** (grey lines) in the PMMA films.

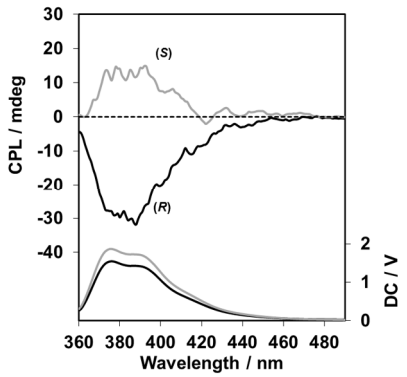

Fig. 10 CPL (upper panel) and PL (lower panel) spectra of (R)-**2** (black lines) and (S)-**2** (grey lines) in PMMA films.

For **1** and **2**, a subtle enhancement in the Φ_F value in the PMMA films compared to Φ_F in the $CHCl_3$ solution was observed due to suppression of thermal deactivation modes because **1** and **2** are embedded into the glassy PMMA matrix. As reported previously, (R)-**3** in PMMA has Φ_F 0.14 and $|g_{em}|$ ~1.4×10^{-3}, which is similar to (R)-**1** and (R)-**2**.[4a,10] It is worth noting that relationships between (R)-**1** and (R)-**3** and between (R)-**2** and (R)-**3** maintain their opposite sign in their CPL spectra: a negative sign for (R)-**1** and (R)-**2**, conversely, a positive sign for (R)-**3**[10].

The CD and UV-Vis spectra of **1** and **2** dispersed in spin-coated PMMA films were measured (Figs 11 and 12). CD and UV-Vis spectral profiles of (R)-**1** and (R)-**2** in PMMA are similar to those observed in the $CHCl_3$ solution at longer wavelengths. The $|g_{CD}|$ values in the first Cotton CD bands of (R)-**1** and (R)-**2** are ~1.9×10^{-3} at 336 nm and ~5.2×10^{-4} at 361 nm, respectively. The CD spectra of (S)-**1** and (S)-**2** in the PMMA films are almost mirror images of those of the corresponding (R)-**1** and (R)-**2**.

The solid-state chiroptical results indicate that the CPL and CD signals in PMMA films originate dominantly from the intramolecular interactions within the isolated molecule itself rather than from intermolecular interactions between multiple molecules. Additionally, the CPL sign even in PMMA can

change in response to the internal axial bonding position of biaryl units.

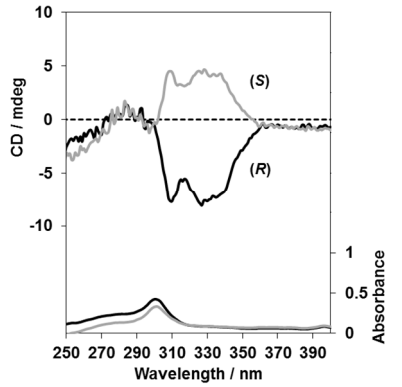

Fig. 11 CD (upper panel) and UV-Vis (lower panel) spectra of (*R*)-**1** (black lines) and (*S*)-**1** (grey lines) in the PMMA films.

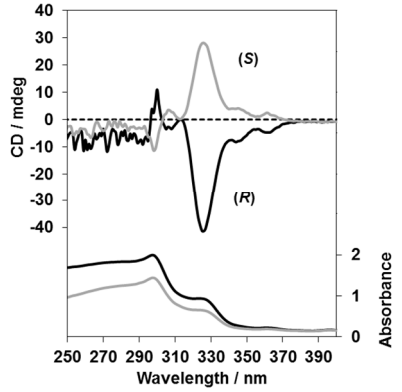

Fig. 12 CD (upper panel) and UV-Vis (lower panel) spectra of (*R*)-**2** (black lines) and (*S*)-**2** (grey lines) in the PMMA films.

Conclusions

Chiral biaryl fluorophores (*R*)-**1** and (*R*)-**2** exhibit fluorescence properties in fluidic $CHCl_3$ solution and glassy PMMA film states. Despite the same axial chirality in the biaryl unit, the CPL and CD signs of the biaryl fluorophores are reversed in both $CHCl_3$ and PMMA film by changing the internal axial bonding position to the biaryl units. These results led to facile control of the CPL sign of the biaryl fluorophores in solution and PMMA states by altering the direction of dipole moments in the chiral biaryl units. Since chiral fluorophores with opposite point chirality are not always accessible, the present knowledge of biaryl fluorophores might provide more flexible ideas in developing novel chiral organic fluorophores. In developing practical chiral fluorescent systems, the facile controllability of chiroptical properties shown in this work is crucial.

Acknowledgements

This study was supported by a Grant-in-Aid for Scientific Research (No. 24550165) from the Ministry of Education, Culture, Sports, Science and Technology (MEXT), Japan, a MEXT-Supported Program for the Strategic Research Foundation at Private Universities, 2014-2018, and the Iketani Science and Technology Foundation. We are thankful to Leigh McDowell (NAIST) for English proofreading our manuscript.

Notes and references

[a] *Department of Applied Chemistry, Faculty of Science and Engineering, Kinki University, 3-4-1 Kowakae, Higashi-Osaka, Osaka 577-8502, Japan. E-mail: (Y.I.) y-imai@apch.kindai.ac.jp.*
[b] *Computational Materials Science Center, National Institute for Materials Science 1-2-1 Sengen, Tsukuba, Ibaraki 305-0047, Japan.*
[c] *Graduate School of Materials Science, Nara Institute of Science and Technology, Takayama, Ikoma, Nara 630-0192, Japan. E-mail: (M.F.) fujikim@ms.naist.jp*

† Electronic Supplementary Information (ESI) available: See DOI: 10.1039/b000000x/

1 (a) J. Shinar, *Organic Light-Emitting Devices,* Springer, New York, Berlin, Heidelberg, 2004; (b) K. Müllen, U. Scherf, *Organic Light-Emitting Devices,* Wiley-VCH, Weinheim, 2006; (c) C. Jeanne, R. Regis, *Dalton. Trans.* 2008, 6865-6876; (d) S. Kappaun, C. Slugovc, J. M. Emil, *Int. J. Mol. Sci.* 2008, **9**, 1527-1547; (e) K. Milan, O. Franc, *Acc. Chem. Res*. 2009, **42**, 235-248; (f) W-Y. Wong, C-L. Ho, *J. Mater. Chem*. 2009, **19**, 4457-4482; (g) K-L. Chan, P. Sonar, A. Sellinge, *J. Mater. Chem*. 2009, **19**, 9103-9120; (h) F. Laquai, Y-S. Park, J-J. Kim, T. Basche, *Macromol. Rapid Commun.*2009, **30**, 1203-1231; (i) C. Wang, J. Zhang, K. Ryu, A. Badmaev, L. G. D. Arco, C. Zhou, *Nano Lett.* 2009, **9**, 4285-4291; (j) M-K.Wei, C-W. Lin, C-C. Yang, Y-W. Kiang, J-H. Lee, H-Y. Lin, *Int. J. Mol. Sci.* 2010, **11**, 1527-1545 and references cited therein.

2 (a) K. E. S. Phillips, T. J. Katz, S. Jockusch, A. J. Lovinger, N. J. Turro, *J. Am. Chem. Soc*. 2001, **123**, 11899-11907; (b) J. E. Field, G. Muller, J. P. Riehl, D. Venkataraman, *J. Am. Chem. Soc*. 2003, **125**, 11808-11809; (c) H. Maeda, Y. Bando, K. Shimomura, I. Yamada, M. Naito, K. Nobusawa, H. Tsumatori, T. Kawai, *J. Am. Chem. Soc*. 2011, **133**, 9266-9269; (d) R. Tempelaar, A. Stradomska, J. Knoester, F. C. Spano, *J. Phys. Chem*., *B* 2011, **115,** 10592-10603; (e) Y. Nakano, M. Fujiki, *Macromolecules* 2011, **44**, 7511-7519; (f) J. Liu, H. Su, L. Meng, Y. Zhao, C. Deng, J. C. Y. Ng, P. Lu, M. Faisal, J. W. Y. Lam, X. Huang, H. Wu, K. S. Wong, B. Z. Tang, *Chem Sci*. 2012, **3**, 2737-2747; (g) Y. Sawada, S. Furumi, A. Takai, M. Takeuchi, K. Noguchi, K. Tanaka, *J. Am. Chem. Soc*. 2012, **134**, 4080-4083; (h) H. Oyama, K. Nakano, T. Harada, R. Kuroda, M. Naito, K. Nobusawa, K. Nozaki, *Org. Lett*. 2013, **15**, 2104-2107; (i) J. Kumar, T. Nakashima, H. Tsumatori, T. Kawai, *J. Phys. Chem. Lett*. 2014, **5**, 316-321; (j) T. Shiraki, Y. Tsuchiya, T. Noguchi, S.-i. Tamaru, N. Suzuki, M. Taguchi, M. Fujiki, S. Shinkai, *Chem. Asian J*. 2014, **9**, 218-222; (k) X. Jiang, X. Liu, Y. Jiang, Y. Quan, Y. Cheng, C. Zhu, *Macromol. Chem. Phys*. 2014, **215**, 358-364; (l) Y. Morisaki, M. Gon, T. Sasamori, N. Tokitoh, Y. Chujo, *J. Am. Chem. Soc*. 2014, **136**, 3350-3353; (m) S. Abbate, G. Longhi, F. Lebon, E. Castiglioni, S. Superchi, L. Pisani, F. Fontana, F. Torricelli, T. Caronna, C. Villani, R. Sabia, M. Tommasini, A. Lucotti, D. Mendola, A. Mele, D. A. Lightner, *J. Phys. Chem. C* 2014, **118**, 1682-1695 and references cited therein.

3 (a) G. A. Hembury, V. V. Borovkov, Y. Inoue, *Chem. Rev.* 2008, **108**, 1-73; (b) Y. Imai, K. Kawano, Y. Nakano, K. Kawaguchi, T. Harada, T. Sato, M. Fujiki, R. Kuroda, Y. Matsubara, *New J. Chem.* 2008, **32**, 1110-1112; (c) N. Nishiguchi, T. Kinuta, Y. Nakano, T. Harada, N. Tajima, T. Sato, M. Fujiki, R. Kuroda, Y. Matsubara, Y. Imai, *Chem. Asian J.* 2011, **6**, 1092-1098; (d) N. Nishiguchi, T. Kinuta, T. Sato, Y. Nakano, H. Tokutome, N. Tajima, M. Fujiki, R. Kuroda, Y. Matsubara , Y. Imai, *Chem. Asian J.* 2012, **7**, 360-366.

4 (a) T. Kinuta, N. Tajima, M. Fujiki, M. Miyazawa, Y. Imai, *Tetrahedron* 2012, **68**, 4791-4796; (b) T. Kimoto, N. Tajima, M. Fujiki, Y. Imai, *Chem. Asian J.* 2012, **7**, 2836-2841; (c) T. Amako, T. Kimoto, N. Tajima, M. Fujiki, Y. Imai, *RSC Adv.* 2013, **3**, 6939-6944; (d) T. Kimoto, T. Amako, N. Tajima, R. Kuroda, M. Fujiki, Y. Imai, *Asian J. Org. Chem*. 2013, **2**, 404-410.

5 Z. Ding, W. E. G Osminski, H. Ren, W. D. Wulff, *Org. Process Res. Dev*. 2011, **15**, 1089-1107.
6 A. D. Becke, *J. Chem. Phys.* 1993, **98**, 5648-5652.
7 M. E. Casida, *Recent Advances in Density Functional Methods*, Vol 1, edited by D. P. Chong, World Scientific, Singapore, 1995.
8 (a) T. H. Dunning Jr., *J. Chem. Phys.* 1989, **90**, 1007-1023; (b) D. E. Woon, T. H. Dunning, Jr. *J. Chem. Phys.* 1993, **98**, 1358-1371.
9 Gaussian 03, Rev. C.02, M. J. Frisch, G. W. Trucks, H. B. Schlegel,G. E. Scuseria, M. A. Robb, J. R. Cheeseman, J. A. Montgomery. Jr, T. Vreven, K. N. Kudin, J. C. Burant, J. M. Millam, S. S. Iyengar, J. Tomasi, V. Barone, B. Mennucci, M. Cossi, G. Scalmani, N. Rega, G. A. Petersson, H. Nakatsuji, M. Hada, M. Ehara, K. Toyota, R. Fukuda, J. Hasegawa, M. Ishida, T. Nakajima, Y. Honda, O. Kitao, H. Nakai, M. Klene, X. Li, J. E. Knox, H. P. Hratchian, J. B. Cross, V. Bakken, C. Adamo, J. Jaramillo, R. Gomperts, R. E. Stratmann, O. Yazyev, A. J. Austin, R. Cammi, C. Pomelli, J. W. Ochterski, P. Y. Ayala, K. Morokuma, G. A. Voth, P. Salvador, J. J. Dannenberg, V. G. Zakrzewski, S. Dapprich, A. D. Daniels, M. C. Strain, O. Farkas, D. K. Malick, A. D. Rabuck, K. Raghavachari, J. B. Foresman, J. V. Ortiz, Q. Cui, A. G. Baboul, S. Clifford, J. Cioslowski, B. B. Stefanov, G. Liu, A. Liashenko, P. Piskorz, I. Komaromi, R. L. Martin, D. J. Fox, T. Keith, M. A. Al-Laham, C. Y. Peng,A. Nanayakkara, M. Challacombe, P. M. W. Gill, B. Johnson, W. Chen, M. W. Wong, C. Gonzalez, and J. A. Pople,; Gaussian, Inc., Wallingford, CT, 2004.
10 T. Kinuta, T. Sato, Y. Nakano, T. Harada, N. Tajima, M. Fujiki, R. Kuroda, Y. Matsubara, Y. Imai, *J. Photochem. Photobiol. A: Chem.* 2011, 134-138.
11 Redrawn based on the original data taken from Ref. 10.
12 (a) T. Amako, T. Harada, N. Suzuki, K. Mishima, M. Fujiki, Y. Imai, *RSC Adv.* 2013, **3**, 23508-23513; (b) Y. Kitayama, T. Amako, N. Suzuki, M. Fujiki, Y. Imai, *Org. Biomol. Chem.* 2014, **12**, 4342-4346.

Cite this: DOI: 10.1039/c0xx00000x

www.rsc.org/xxxxxx

ARTICLE TYPE

Graphical Abstract

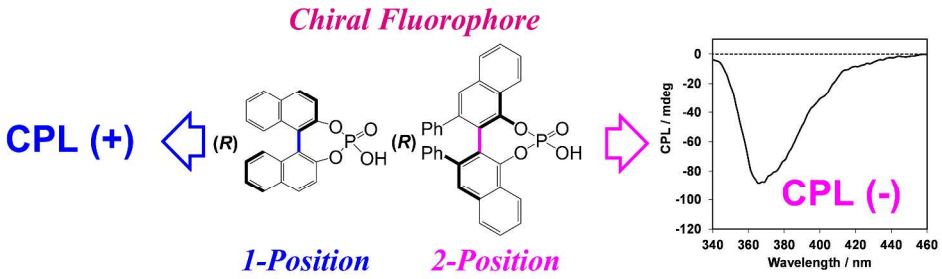

The signs of circularly polarised luminescence and circular dichroism of chiral biaryl organic fluorophores in the $CHCl_3$-dissolved state (solution state) and the PMMA-film-dispersed state (solid state) were successfully controlled by modifying the internal axial chirality and the axial bonding position of biaryl units.